

SMMR data used for this map. This influence occurs out to approximately 1000 km from major land areas. Implementation of a side-lobe correction algorithm (12) will reduce this distance to approximately 300 km (two resolution cells) as tests on limited Seasat data sets have indicated.

These results indicate that microwave radiometers orbiting the earth can measure SST with a root-mean-square sensitivity of 1.2°C or better. Better results will probably be possible with improved instrument calibration, sensitivity, and retrieval algorithms.

R. HOFER*
E. G. NJOKU
J. W. WATERS

Earth and Space Sciences Division,
Jet Propulsion Laboratory,
California Institute of Technology,
Pasadena 91109

References and Notes

1. T. P. Barnett, W. C. Patzert, S. C. Webb, B. R. Bean, *Bull. Am. Meteorol. Soc.* **60**, 197 (1979). However, work is under way to reduce these limitations: M. T. Chahine, in *Remote Sensing of Atmospheres and Oceans*, A. Deepak, Ed. (Academic Press, New York, 1980), p. 411; E. P. McClain, in *Oceanography from Space* (proceedings of the COSPAR/SCOR/IUCRM symposium, Venice, Italy, 1980) (Plenum, New York, in press), p. 73; P. Y. Deschamps and T. Phulpin, *Boundary-Layer Meteorol.* **18**, 131 (1980).
2. D. H. Staelin, *Proc. IEEE* **57**, 427 (1969); K. Tomiyasu, *ibid.* **62**, 86 (1974); E. Schanda, in *Ecological Studies*, vol. 18, *Remote Sensing for Environmental Sciences*, E. Schanda, Ed. (Springer, Berlin, 1978), p. 187.
3. D. H. Staelin, A. H. Barrett, J. W. Waters, F. T. Barath, E. J. Johnston, P. W. Rosenkranz, N. E. Gaut, W. B. Lenoir, *Science* **182**, 1339 (1973); D. H. Staelin, P. W. Rosenkranz, F. T. Barath, E. J. Johnston, J. W. Waters, *ibid.* **197**, 991 (1977); D. H. Staelin, K. F. Kunzi, R. L. Pettyjohn, R. K. L. Poon, R. W. Wilcox, J. W. Waters, *J. Appl. Meteorol.* **15**, 1204 (1976); T. T. Wilheit, A. T. C. Chang, M. S. V. Rao, E. B. Rodgers, J. S. Theon, *ibid.* **16**, 551 (1977); J. W. Waters, K. F. Kunzi, R. L. Pettyjohn, R. K. L. Poon, D. H. Staelin, *J. Atmos. Sci.* **32**, 1953 (1975); A. T. C. Chang and T. T. Wilheit, *Radio Sci.* **14**, 793 (1979); T. T. Wilheit, *Boundary-Layer Meteorol.* **13**, 277 (1978); ———, A. T. C. Chang, A. S. Milman, *ibid.* **18**, 65 (1980); W. J. Campbell, R. O. Ramseier, H. J. Zwally, P. Gloersen, *ibid.*, p. 99; K. F. Kunzi, A. D. Fisher, D. H. Staelin, J. W. Waters, *J. Geophys. Res.* **81**, 4965 (1976).
4. T. T. Wilheit, *IEEE Trans. Geosci. Electron.* **GE-17**, 244 (1979).
5. E. G. Njoku, J. M. Stacey, F. T. Barath, *IEEE J. Oceanic Eng. OE-5*, 100 (1980).
6. R. Hofer and E. G. Njoku, *IEEE Trans. Geosci. Remote Sensing*, in press. Other algorithms have also been developed; for example: P. W. Rosenkranz, *Radio Sci.* **13**, 1003 (1978); T. T. Wilheit and A. T. C. Chang, *ibid.* **15**, 525 (1980); F. J. Wentz, in *Seasat Gulf of Alaska Workshop Report I* (internal publication 622-101, Jet Propulsion Laboratory, Pasadena, Calif., 1979), pp. 8-19.
7. P. N. Swanson and A. L. Riley, *IEEE J. Oceanic Eng. OE-5*, 116 (1980).
8. J. A. Renner, Ed., *Fishing Information*, produced monthly by the National Oceanic and Atmospheric Administration National Marine Fisheries Service, Southwest Fisheries Center, La Jolla, Calif.
9. V. J. Cardone, in *Seasat Gulf of Alaska Workshop II Report* (internal publication 622-107, Jet Propulsion Laboratory, Pasadena, Calif., 1979), pp. 2-6.
10. J. P. Peixoto and A. R. Crisi, *Hemispheric Humidity Conditions During the IGY* (Department of Meteorology, Massachusetts Institute of Technology, Cambridge, 1965), p. 17.

11. W. B. White and R. L. Bernstein, *J. Phys. Oceanogr.* **9**, 592 (1979).
12. E. G. Njoku, E. J. Christensen, R. E. Cofield, *IEEE J. Oceanic Eng. OE-5*, 125 (1980).
13. R. Hofer and E. G. Njoku, in preparation.
14. We thank R. Bernstein of the Scripps Institution of Oceanography for providing the XBT comparison data, J. Kitzis and S. Kitzis for major programming assistance, and the Seasat project personnel for providing the SMMR data. R. Bernstein, M. Chahine, and H. Press made useful comments on the manuscript. R. H. thanks the National Research Council for pro-

viding his resident research associate position during this research. The research described in this report was supported in part by the National Academy of Sciences and was carried out at the Jet Propulsion Laboratory, California Institute of Technology, sponsored by the Oceanic Process Branch and the Climate Program Office, Office of Space and Terrestrial Applications, under NASA contract NAS 7-100.

* Present address: CIBA-GEIGY AG, Basel, Switzerland.

24 December 1980; revised 20 March 1981

Hydrovolcanic Explosions: The Systematics of Water-Pyroclast Equilibration

Abstract. *The initial contact of external water with erupting magma and the mass ratio of water to magma govern the development of hydrovolcanic phenomena. The phase relations of water within the runout system and the separation of vapor or liquid from the pyroclasts explain gradational transitions between some pyroclastic flows, base surges, mud hurricanes, mudflows, and sheetfloods.*

Hydrovolcanism refers to volcanic phenomena produced by the interaction of magma or magmatic heat with an external source of water, such as a surface body or an aquifer. There is a complete spectrum of activity, from hydro-magmatic to purely magmatic. Most active volcanoes exhibit at least limited periods of hydrovolcanic activity, and it is the dominant type of activity for some volcanoes. Shallow subaqueous eruptions commonly produce hydrovolcanic explosions with ash showers and base-surge clouds, as at Surtsey (1964-1965), Taal (1965), and Capelinhos (1957). Less widely recognized is the subsurface involvement of external water in the explosive eruptions of stratovolcanoes such as Vesuvius (1).

The 1980 activity of Mount St. Helens has focused attention on the destruction consequent on hydrovolcanic phenomena. This can include debris flows, pyroclastic flows, base surges, mud hurricanes, mudflows, and flash floods (2). Even basaltic shield volcanoes exhibit rare hydrovolcanic phases, such as the 1790 and 1924 base-surge eruptions of Kilauea (3). This report, which incorporates new data obtained in the field and experimentally (4), presents the systematics of water-pyroclast (5) interactions as a foundation for a quantitative model of hydrovolcanic activity.

Hydrovolcanic explosions (6) produce phenomena that are governed by the initial mixing of magma with water from an external source and the subsequent separation of the entrained water (vapor or liquid) and pyroclasts during eruption and emplacement. The important factors that control the expansion, collapse, and lateral displacement of the system include the mass ratio of water to pyroclasts, the physical state of the water (supercritical fluid, superheated steam, multiphase fluid, or liquid), and the density of the mixture of fluid and particulates.

The initial contact of water and magma, in which thermal energy of the magma is transferred into mechanical energy of the fluid-particulate mixture, determines the subsequent development of hydrovolcanic phenomena. We have conducted a series of experiments to test the effect of the water/magma mass ratio on the efficiency of energy conversions. Data on vapor explosions (7, 8) permitted the design of a series of scale-model experiments [involving a large chamber containing mixtures of thermite and water (4)] which were used to make first-

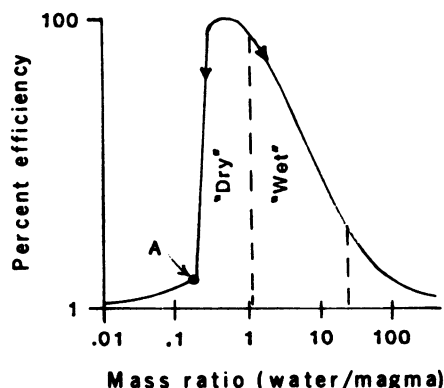


Fig. 1. The conversion efficiency of thermal energy to mechanical energy as a function of the water/magma ratio for the thermite and water system (4). The thermal energy per unit mass of thermite is approximately three times that of basalt. Hence the ratio scale must be multiplied by an appropriate factor (3 or 4) to model volcanic systems. With increasing water/magma ratio, the onset of superheating and explosive fragmentation occurs at point A.

order estimates of energy partition in the system (Fig. 1).

The efficiency of energy transfer is largely controlled by the water/magma ratio, the amount of superheating of the water, and the extent of fragmentation of the magma. Increased magma fragmentation, and hence particle surface area, increases the amount of energy transferred, which reaches a maximum at the point where water has absorbed as much heat as possible prior to spontaneous, homogeneous boiling. Under a large confining pressure, the maximum heat energy absorbed by the water will be at the limit of superheating, the temperature of which depends on the confining pressure (9). The influx of magma and water into the mixing space may help to determine whether the ensuing vaporizations produce pulsating or steady eruptions.

The energy partition diagram (Fig. 1) illustrates a range of hydrovolcanic phenomena. If the water/magma ratio is low (below point A in Fig. 1), then water plays only a minor role in determining eruption characteristics, and magmatic gases may produce lava or pumice-fall (scoria-fall) eruptions. Water/magma ratios above point A are accompanied by a drastic increase in superheating, energy-transfer efficiency, and magma fragmentation and can produce highly energetic explosions accompanied by vapor-expanded pyroclastic flows and dry base surges (10). An increase in water/magma ratio above 1.0 produces a decrease in superheating and mechanical energy, leading to less explosive eruptions with wet base surges, mud hurricanes, and lahars (11). A natural division of transport into dry and hot (superheated steam matrix) or cold and wet (condensing steam matrix) can be directly related to the initial mixture ratio prior to explosion.

To evaluate observed eruption phenomenology, we present a general model that includes the six gradational stages of entrainment and expulsion of water commonly observed during periods of hydrovolcanic activity (Fig. 2). The establishment of each stage depends on several factors, and a single explosion, or a series of explosions, rarely exhibits all six stages in succession.

Stage 1, the initial contact of water and magma, is the principal factor in the development of every hydrovolcanic eruptive impulse. Violent mixing leading to a fuel-coolant type of explosion (7, 12) is responsible for many shallow subaqueous eruptions (4, 8). However, incorporation of large quantities of external water into fragmental magma is not limited to near-surface locations. It occurred at

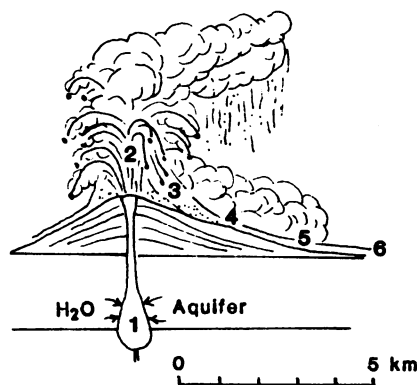


Fig. 2. Schematic diagram of a fully developed hydrovolcanic system (20) showing six stages of water-pyroclast interaction: 1, initial mixing of water and magma; 2, explosive decompression of steam; 3, separation of steam and pyroclasts from the column; 4, runout of dry (superheated) mixtures; 5, runout of wet (condensing steam) mixtures; and 6, sheetfloods. The last three stages may occur at any distance from the vent or they may be absent.

depths as great as 5 km during the Plinian eruptions of Vesuvius (1).

Stage 2, venting of the fragmented magma and superheated water, is related to the explosive transition from superheated water into expanded vapor. Vaporization waves (13) transmitted from the zone of mixing may produce a resonance that causes an oscillation in the intensity of explosions. Such oscillations can control mixing rates. In contrast to magmatic systems that produce a strong gas-thrust column above the vent, the explosive expansion of a superheated steam mixture as it reaches the low confining pressure at the surface can produce a lateral "directed" blast common in hydrovolcanic eruptions. The degree of expansion of the volcanic column above the vent is a function of the levels of water superheating and magma fragmentation—analogueous to the expansion of columns in dominantly magmatic systems (14).

Stage 3 marks the separation of pyroclasts and vapor from the vertical transport stream in the eruptive column. Pyroclasts elutriated from the top of the column are dispersed by atmospheric winds and eventually return to the earth as fallout. Fragments too large to be supported in the column may be ejected outward along ballistic paths. Gravitational instability in the column may result in massive collapse (15). Surge blasts are initiated either by short-lived explosions produced by near-surface decompression of superheated steam or by compressional waves generated by column collapse.

Stage 4 involves the runout from the

vent of pyroclastic clouds with a supporting matrix of steam and air. Due to their increased fluidity, highly inflated pyroclastic flows with initial low concentrations of particles tend to move farther from the vent before coming to rest (16). Pyroclastic flows and surge clouds containing superheated steam are considered hot and dry. During transport the steam separates from the particles and escapes so that the cloud density increases with time. Deposits so produced remain stable and dry.

Stage 5 follows the transition of steam to water during the runout of particulate avalanches and clouds. The initial degree of water superheating in stage 1 is the critical factor in the formation of water-rich flows. If the steam is highly superheated, much of it may escape from pyroclast avalanches and clouds prior to condensation, resulting in a dry deposit. However, if condensation occurs while the cloud still has a high steam content, the particles become nucleation centers and the resulting deposits are wet. These local nucleation centers may grow rapidly, aided by electrostatic forces, forming accretionary lapilli. If sufficient water is present, wet aggregates may become remobilized as lahars on the lower flanks of the volcano. This can occur through the addition of surface water, dilation in response to earthquakes, or percolation of entrained water through the porous deposits to the toes of flows. Under proper conditions, hot, dry pyroclastic flows or surges could grade imperceptibly into cold, wet flows, slurries, and eventually mudflows or lahars.

Stage 6 occurs when wet flows slow to a halt, but water continues to separate from the particulates and move even farther from the volcano as floods. Separation could take place while a wet slurry is moving so that the massive, poorly sorted basal layer is covered by cross-stratified, better sorted deposit formed by sheetwash. In other cases, separation of the water-rich sheetwash or flash flood from wet pyroclastic-flow, base-surge, or mudflow deposits could occur after the primary unit comes to rest, as may have happened during the 18 May 1980 eruption of Mount St. Helens (2).

Abundant evidence from eruptions supports this model of a spatial transition from proximal, hot, dry deposits (stage 4) to distal, cold, wet emplacement (stages 5 and 6). The 1968 eruptions of Mayon (17) and the 1976 eruptions of Santaguito (18) are documented examples of dry, hot pyroclastic flows or surges that were closely followed by cold, wet lahars or flash floods. In some eruptions the system becomes so flooded

with water during stage 1 that mud hurricanes, lahars, or sheetfloods may be the only phenomena observed. These may be only steam-blast eruptions like the 1976 eruptions of La Soufrière (19), which at times emitted lahars directly from the venting fissures (20).

In still other cases, a gradual increase in water/magma mixing ratios during stage 1 provides a change in eruptive characteristics with time. The Plinian deposits from the A.D. 79 eruption of Vesuvius (1) provide an excellent example of this type of progression. The dominantly magmatic initial pumice-fall phase went through an alternating transition into dry, hot base surges followed by dry, hot pyroclastic flows which reflected a progressive increase in the water/magma ratio in the chamber. By the late stages of the eruption, water greatly exceeded magma so that mud hurricanes, lahars, and steam explosions ended the cycle. The history of this eruption can be traced in Fig. 1 by considering a regular increase in the water/magma ratio during the 18 hours of activity. Low ratios (less than 1) during the Plinian phase increased to moderate levels (near 3) during the base-surge and pyroclastic-flow phases and to very high values (perhaps up to 30) during the final period of mud hurricanes and lahars.

Another documentation of this model is found in typical tuff cones, which are composed of a layer of explosion breccia, overlain by dry, hot base-surge deposits, in turn covered by cold wet-surge beds and lahars (21). This progression could likewise be interpreted as a result of increasing water/magma ratios from less than 3 to more than 3 as the vent widens during eruption (22).

Hydrovolcanic phenomena are common, and we believe that the use of our model will lead to a better understanding of the related deep processes, eruption phenomena, and surficial deposits.

MICHAEL F. SHERIDAN
KENNETH H. WOHLTZ

Department of Geology,
Arizona State University,
Tempe 85281

References and Notes

1. M. F. Sheridan, F. Barberi, R. Santacroce, M. Rosi, *Nature (London)* **289**, 282 (1981).
2. Mount St. Helens is still active at this writing. The volume of water produced in the floods was greater than the available surface water that could be incorporated in the deposit. Therefore a source from within the volcano is postulated. Our data are based on news reports, informal scientific communications, photographs, discussions with scientists who are studying the volcano, and videotapes taken by Michael Malin.
3. T. A. Jagger, *Hawaii. Volcano Obs. Fourth Spec. Rep.* (1949).
4. K. H. Wohletz, thesis, Arizona State University, Tempe (1980); *Eos* **61** (No. 6), 66 (1979).
5. Pyroclasts are the individual crystals, crystal fragments, glass fragments, and rock fragments

- generated by disruption as a direct result of volcano action [R. Schmid, *Geology* **9** (No. 1), 41 (1981)].
6. The term explosion is here used to denote the rapid emission of vapor and particles from a vent, as opposed to the slow evolution of lava. Volcanic explosions, which rarely develop on the time scale of thermal chemical explosions, may be single short-lived blasts, episodic bursts, or sustained periods of emission lasting hours to days.
 7. R. S. Peckover, D. J. Buchanan, D. E. Ashby, *Nature (London)* **245**, 307 (1973).
 8. S. A. Colgate and T. Sigurgeirsson, *ibid.* **244**, 552 (1973).
 9. R. C. Reid, *Am. Sci.* **64**, 146 (1976).
 10. Pyroclastic flows include denser-than-air avalanches, streams, and flows receiving their initial energy from volcanic eruptions and traveling with near steady-state motion (15). Base surges are dilute clouds that rapidly dissipate their mechanical energy; most result from pulsating hydrovolcanic eruptions. Dry base surges are emplaced above the condensation temperature so that superheated steam is mostly lost prior to emplacement.
 11. Wet base surges are emplaced below the condensation temperature so that a film of water has condensed on the transported particles, often leading to the development of accretionary or ash-armed lapilli. Mud hurricanes are wet ash-laden blasts that travel at very high velocities and are capable of leaving thick deposits on

- vertical surfaces. Accretionary lapilli and bubble-filled ash layers (vesicular tuffs) are common products. Lahars are volcanic mudflows.
12. Sandia Laboratories, *Core-meltdown Experimental Review* (SAND-74-0382, Sandia Laboratories, Albuquerque, N.M., 1975).
 13. F. D. Bennett, *J. Geophys. Res.* **77**, 5755 (1972).
 14. L. Wilson, *Geophys. J. R. Astron. Soc.* **45**, 543 (1976).
 15. R. S. J. Sparks, L. Wilson, G. Hulme, *J. Geophys. Res.* **83**, 1727 (1978); R. S. J. Sparks and L. Wilson, *J. Geol. Soc. (London)* **132**, 441 (1976).
 16. M. F. Sheridan, *Geol. Soc. Am. Mem.* **180**, 125 (1979).
 17. J. G. Moore and W. G. Melson, *Bull. Volcanol.* **33**, 600 (1969).
 18. W. I. Rose, Jr., T. Pearson, S. Bonis, *ibid.* **40**, 1 (1977).
 19. M. F. Sheridan, *ibid.*, in press.
 20. K. H. Wohletz and B. M. Crowe, *Geol. Soc. Am. Abstr. Programs* **10**, 154 (1978).
 21. K. H. Wohletz, *ibid.* **11**, 543 (1979).
 22. _____ and M. F. Sheridan, in preparation; M. F. Sheridan and K. H. Wohletz, *Eos* **61**, 1142 (1980).
 23. This work benefited from discussions and reviews by J. Fink, M. Malin, and E. Stump. Partially supported by United States-Italy NSF grant INT-7823984 and NASA Office of Planetary Geology grant NSG-7642.

17 October 1980; revised 17 February 1981

Soil as a Sink for Atmospheric Carbon Monoxide

Abstract. *The rate of carbon monoxide oxidation by soil increased with increasing carbon monoxide concentration in the gas phase, in line with Michaelis-Menten kinetics. Rates of carbon monoxide oxidation were determined for 20 soils at 0°, 10°, 20°, and 30°C. The observed oxidation rates were used to calculate a global soil uptake rate of atmospheric carbon monoxide of 4.1×10^{14} grams per year, which is slightly less than the amount of carbon monoxide believed to be produced annually as a result of fossil fuel combustion.*

Much attention has been focused on the possible perturbation of the atmospheric CO cycle by anthropogenic CO emissions. Seiler (1) estimated that the amount of CO produced from fossil fuel combustion is 6.4×10^{14} g/year, a large value by comparison with the 7.4×10^{14} g of CO currently in the atmosphere (2). Crutzen *et al.* (3) suggested that biomass burning, which results largely from man's activities, produces more CO than fossil fuel combustion.

The effect of anthropogenic CO production of this magnitude on the atmospheric cycle depends to a great extent on the ability of removal mechanisms to maintain present atmospheric concentrations of CO (1, 4). The main sinks for atmospheric CO are believed to be the reaction of tropospheric hydroxyl radicals with CO and the oxidation of CO by soil (1, 4). Ingersoll *et al.* (5) estimated the global soil uptake of CO to be 1.4×10^{15} g/year. This value was derived from field studies of soils at 59 sites in North America that were exposed to 100 parts per million by volume (ppmv) of CO. Based on measurements of a few European soils in the laboratory, Seiler (1) estimated the global uptake of CO by soil to be 5.0×10^{14} g/year. We report

here the effect of CO concentration on the rate of its destruction by soil, and we estimate the magnitude of CO uptake by soil on a global basis from uptake measurements on 20 soils.

We measured the effect of the CO concentration on the rate of its oxidation by a modification of the method of Pramer and Schmidt (6). Portions (5.0 g) of Williamson silt loam (pH 5.8, 2.6 percent organic matter, 22 percent moisture content) were placed in 25-ml Erlenmeyer flasks. The flasks were sealed with serum stoppers, and varying amounts of a ^{12}CO - ^{14}CO mixture (9:1 ratio by volume) were added to the flasks by means of a gas-tight syringe. The flasks were incubated for 30 minutes at 23°C, after which the $^{14}\text{CO}_2$ formed from ^{14}CO was trapped and measured. We obtained the ^{12}CO - ^{14}CO mixture by dehydrating $\text{H}^{12}\text{COONa}$ and $\text{H}^{14}\text{COONa}$ (New England Nuclear, specific activity of 52 mCi/mmol) with concentrated H_2SO_4 (7). Details of these methods and data showing that CO oxidation in soil results from microbial activity have been reported (8).

To study CO oxidation at different temperatures, samples of surface soils from sites in the eastern United States